Energy & Environmental Science

Accepted Manuscript

ROYAL SOCIETY OF CHEMISTRY

www.rsc.org/ees

Journal Name

COMMUNICATION

Self-terminated electrodeposition of iridium electrocatalysts

Sang Hyun Ahn,[a] Haiyan Tan,[a] Mareike Hansch,[a] Yihua Liu,[a] Leonid A. Bendersky[a] and Thomas P. Moffat[a,*]

Received 00th January 20xx,
Accepted 00th January 20xx

DOI: 10.1039/x0xx00000x

www.rsc.org/

A simple electrochemical process for submonolayer deposition of ultrathin catalytic Ir films is demonstrated. This method enables effective utilization of one of nature's rarest elements while different substrates facilitate the exploration of promising bimetallic catalysts for a sustainable hydrogen economy. Semi-coherent Ir films were deposited on Au, Pt and Ni substrates using K_3IrCl_6-Na_2SO_4-H_2SO_4 electrolytes operated between 40 °C and 70 °C. However, the deposition reaction is quenched at the onset of H_2 production where adsorbed H blocks the reduction of $IrCl_{6-x}H_2O_x^{3-x}$ to Ir. The electrode can be reactivated for further deposition by pulsing the potential to more positive values where adsorbed H is oxidized. The electrocatalytic activity of ultrathin Ir and Pt films, and combinations thereof, were examined as function of the number of self-terminating deposition pulses. The ultrathin films match or exceed the best reported activity metrics for hydrogen oxidation in alkaline media and oxygen evolution in acid.

Realization of a hydrogen economy depends on catalyzed water electrolysis for energy storage and its reverse reaction for power generation though fuel cells. Iridium and its oxides are among the most active and durable catalysts for water splitting in acid while recent work indicates that Ir may be the best elemental catalyst for hydrogen oxidation in alkaline media.[1-4] However, the crustal abundance of Ir places it among the scarcest elements and subjects it to significant price instability when employed in emerging technologies. Commercialization of water electrolysis and low temperature fuel cells is constrained by the cost and durability of existing Pt-group metal electrocatalysts while the overpotential losses associated with water spitting and related reactions remain a significant barrier to the development of sustainable renewable energy technologies.

To address these challenges two strategies are being explored, namely, enhanced catalytic performance by alloying and minimization of Pt-group metal loading by using architectures that maximize the surface area to volume ratio of expensive constituents. These strategies merge when material minimization is facilitated by forming ultrathin Pt-group metal overlayers on conducting substrates, where the combination of ligand, strain, ensemble and/or alloying interactions associated with the bimetallic surface may offer enhanced reactivity. Several chemical and electrochemical deposition schemes have been developed for depositing thin Pt overlayers. Gas phase atomic layer deposition (ALD) processes have been indentified for several Pt-group metals including Ir but they tend to be slow and involve expensive equipment.[5] In contrast, a "wet" form of ALD based on self-terminated electrodeposition provides a simple and rapid means for controlled deposition of Pt whereby film growth is quenching by adsorbed hydrogen.[6] Using this method sub-monolayer Pt films deposited on Ni yielded among the highest reported values for electrocatalytic hydrogen evolution in alkaline solution.[7]

Beyond catalysis, Ir is noteworthy for its favorable mechanical and chemical properties at high temperatures. However, its high melting point and hardness makes thermo-mechanical processing difficult and has stimulated interest in other fabrication processes such as electrodeposition. Many of these studies start with Ir^{4+} species since Ir^{3+} d^6 complexes are among the most inert to ligand exchange known.[8] A recent study using a H_2IrCl_6-H_2SO_4 electrolyte at room temperature demonstrated the formation of a ≈5 nm thick nanoporous Ir film although it required 2 hours to form.[9] No voltammetric signature of the deposition process was observed although extended polarization at four different potentials revealed a maximum growth rate coincident with the H underpotential deposition (H_{UPD}) region. Ir^{3+} reduction was proposed to be catalyzed by H_{UPD} species with the highest deposition rate corresponding to a fractional H_{UPD} coverage close to 0.5 of a monolayer. A subsequent investigation examining deposition from $IrCl_3$-H_2SO_4 revealed similar behavior although the

[a] Materials Measurement Laboratory, National Institute of Standards and Technology, 100 Bureau Drive, Gaithersburg, Maryland 20899, United States.
† Footnotes relating to the title and/or authors should appear here.
Electronic Supplementary Information (ESI) available: [details of any supplementary information available should be included here]. See DOI: 10.1039/x0xx00000x

current efficiency was reported to be quite poor.[10] The present work revisits electrodeposition of Ir from Ir^{3+} chloro-complexes, illustrating the generality of self-terminated electrodeposition and its application to the formation of Ir clusters and ultrathin films on Au, Pt and Ni substrates via pulsed potential deposition. The utility of these materials as catalyst for reactions central to a hydrogen economy is demonstrated.

Ir electrodeposition was studied using a K_3IrCl_6-Na_2SO_4-H_2SO_4 electrolyte between pH 1.5 and pH 6.5 (Fig. 1a-d). Deposition on Au is thermally activated with development of a well-defined current peak near −0.80 V_{SSE} at temperatures above 40 °C (Fig. 1a). At more negative potentials the current decreases due to quenching of Ir deposition. Self-termination occurs with the onset of hydrogen production followed by diffusion limited proton reduction below −0.85 V_{SSE}. The same processes occur in pH 1.5 with quenching of Ir growth coincident with the onset of hydrogen evolution, ≈−0.70 $V_{SSE,}$ on the Ir covered Au electrode (Fig. 1b). Comparison to Ir voltammetry in the supporting electrolyte reveals overlap between the maximum deposition current and the H_{UPD} regime observed on Ir in the absence of dissolved Ir^{3+}. Similar phenomenon is evident in pH 6.5 (Fig. S1a). Studies using Ir single crystals demonstrate that H_{UPD} waves convolve anion desorption and H adsorption.[11-15]

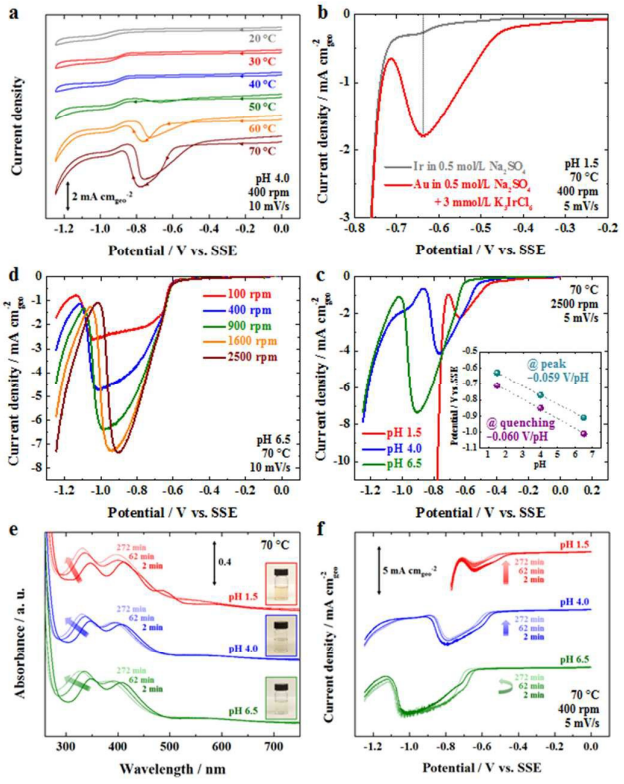

Fig. 1 Self-terminated Ir electrodeposition on Au RDE in 3 mmol/L K_3IrCl_6-0.5 mol/L Na_2SO_4-x mol/L H_2SO_4. (a) Ir deposition is thermally activated. (b) Ir deposition is quenched at the onset of hydrogen evolution. (c) Ir deposition and quenching depends on pH consistent with proton coupled charge transfer reaction. (d) For neutral pH the Ir deposition peak and quenching potentials depend on hydrodynamics. (e) Evolution of Uv-vis spectra for electrolytes at 70 °C. Inset: photographs of the as-prepared electrolytes and (f) the corresponding voltammograms for Ir deposition.

Superposition of Ir deposition and anion desorption/proton adsorption suggest that metal deposition is associated with disruption and desorption of the anion adlayer while formation of a complete H_{UPD} layer terminates Ir deposition. The inverse correlation between H_{UPD} coverage and the metal deposition rate contradicts previous assertions of a catalytic interaction.[9,10]

Ir nucleation on Au is hindered as evident in the scan rate dependence of the onset of deposition in pH 4.0 (Fig. S1b). The onset potential decreases with pH while the peak current increases (Fig. 1c). At low Ir^{3+} concentrations and slow electrode rotation rates the peak deposition current is a monotonic function of the Ir^{3+} flux. However, the peak current saturates for rotation rates above 1600 rpm (Fig. 1d, S1c) reflecting dominance by surface processes. In contrast to pH 4.0 (Fig. S1c), quenching of Ir deposition in pH 6.5 (Fig. 1d) is influenced by mass transport. For the slowest rotation speed a broad deposition wave develops prior to termination of Ir growth at −1.04 V_{SSE}. With increasing rotation speed quenching occurs at more positive potentials and the overall deposition wave is more symmetric. At 2500 rpm the peak potential shifts −0.059 V/pH (Fig. 1c) consistent with a proton coupled charge transfer controlled reaction. Reactivation of the deposition process occurs during the return voltammetric sweep (Fig. 1a, S1d). Ir nucleation and growth kinetics were also examined by chronoamperometry. The steady-state sampled current at modest overpotentials is congruent with the voltammetric results in pH 4.0 (Fig. S2a-d) while in pH 6.5 a lag in quenching is apparent for the negative going sweep (Fig. S3a-d).

Speciation of Ir^{3+} complexes in the as-prepared electrolytes and during electrolysis was examined by Uv-visible absorption spectroscopy. At room temperature octahedral $IrCl_6^{3-}$ is relatively inert to water exchange however, at 70 °C ligand exchange is evident by color change and evolution of the $IrCl_{6-x}(H_2O)_x^{3-x}$ spectra shown in Fig. 1e. Likewise, a multiplicity of Ir^{3+}/Ir^{4+} redox states is evident with aging as evident by cyclic voltammetry (Fig. S4).[16-19] Spectra for aged Ir^{3+} electrolytes were quite similar although a small quantity of Ir^{4+} species was initially present in the pH 1.5 solution due to homogenous reaction between Ir^{3+} and O_2 (Fig. S6-S10). Importantly, the essential characteristics of Ir deposition are not significantly altered by aging of the Ir^{3+} precursors (Fig. 1f). However, when the supporting electrolyte is changed from 0.5 mol/L Na_2SO_4 to 3.0 mol/L NaCl, no Ir deposition is observed at 70 °C (Fig. S11). The high Cl^- concentration stabilizes the chloro-complexes and supports formation of a saturated Cl^- adlayer on the electrode surface. Since $IrCl_6^{3-}$ is the dominant complex in freshly prepared 0.5 mol/L Na_2SO_4 and metal deposition still occurs at 70 °C, adsorbed Cl^- must serve as the key inhibitor of Ir nucleation on Au by blocking adsorption of Ir^{3+} species. Similarly, a rapid increase in Cl^- from 0.01 mol/L to 0.5 mol/L results in quenching of Ir deposition while re-equilibration of chloro-complexes requires a more extended time period (not shown).

Thermal activation of Ir deposition was also examined by thermally cycling the electrolyte. Moving between 70 °C and 20 °C the reaction is turned on and off with little correlation to

the Uv-vis spectral positions of the evolving Ir^{3+} species, although the molar absorptivity changes measurably with temperature (Fig. S12a,b). Analysis of Ir deposition in Fig. 1a indicates an activation energy of (29.5 ± 0.9) kJ/mol (Fig. S12c,d).

Thick Ir films may be grown at potentials within the deposition wave (Fig. S13) however, the present work is focused on pulsed potential deposition whereby the self-terminating character of Ir deposition is used to form ultrathin films. Submonolayer thickness control is attained by stepping to potentials, E_{dep}, where deposition is quenched (Fig. 2a). X-ray photoelectron spectroscopy (XPS) was used to evaluate the amount of Ir deposited on Au-seeded Si wafer fragments. The Ir 4f/Au 4f intensity ratio for one deposition pulse yields an effective Ir thickness of (0.085 ± 0.028) nm based on a uniform overlayer model.[20] A complete monolayer of Ir(111) corresponds to 0.2216 nm thus one deposition pulse gives Ir clusters or islands that cover 25 % to 50 % of the surface. Alternatively, a fractional surface coverage scaled XPS model gives 0.42 ± 0.11 for one layer thick Ir islands or 0.23 ± 0.06 if the islands are two layers in thickness.[21] The coverage is essentially independent of pH (1.5 to 6.5) and deposition time (1 to 100) s. Additional deposition occurs beyond 100 s although the slower growth rate suggests a different secondary process is operating (Fig. S14a). The thickness was insensitive to the deposition potential provided it was below the reversible hydrogen potential (Fig. S14b). For growth times below 100 s coverage is a weak function of the bulk Ir^{3+} concentration (Fig. S14c). Deposition on other substrates, i.e., nickel, was briefly examined as detailed in the supplement (Fig. S15).

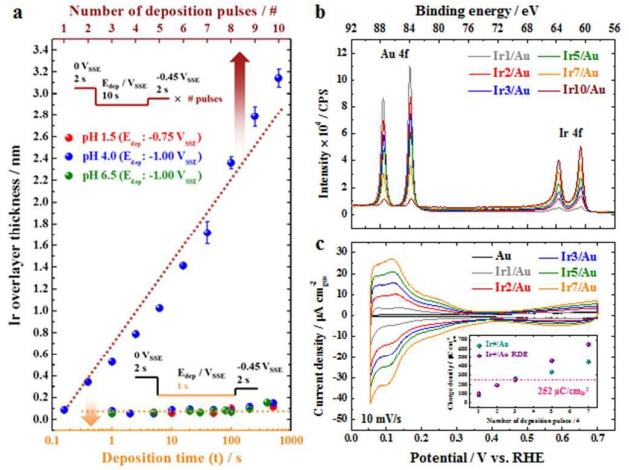

Fig. 2 Spectroscopic and electrochemical characterization of ultrathin Ir films grown on Au-seeded Si wafer by multi-pulse deposition in 3 mmol/L K_3IrCl_6-0.5 mol/L Na_2SO_4-x mol/L H_2SO_4 electrolyte at 70 °C. (a) XPS-derived Ir overlayer thickness is dependent on deposition time and number of pulses but independent of pH. Data points are averaged from at least 3 different regions of individual specimens and the error bars represent the standard deviation of the measurments. (b) Au 4f and Ir 4f XPS spectra for Ir films grown using multi-pulse deposition from a pH 4.0 electrolyte. (c) Cyclic voltammetry of Ir multilayers in Ar-purged 0.5 mol/L H_2SO_4. Inset: calculated H_{UPD} charge density for Ir deposits grown on Au-seeded Si wafer and Au RDE. The charge density corresponds to one-half of the total integrated charge passed between (0.05 and 0.40) V_{RHE}.

Thicker Ir films are deposited using a multi-pulse sequence where the freshly quenched surface is reactivated by stepping to −0.45 V_{SSE} to oxidize adsorbed H immediately prior to each deposition pulse. This method is analogous to atomic layer deposition where pulsed potential, rather than reactant exchange, is used to modulate the interface chemistry as recently demonstrated for Pt.[5,6] Representative potential pulse train and current response for a pH 4.0 electrolyte are given in Fig. S16. XPS reveals a monotonic increase in the Ir 4f/Au 4f ratio with the number of deposition pulses (Fig. 2b), while the Ir 4f binding energy is congruent with its metallic form. Quantitative analysis using a simple Ir overlayer model yields a linear increase in thickness from (0.343 ± 0.012) nm (2 pulses deposition) to (3.143 ± 0.083) nm (10 pulses deposition) (Fig. 2a).[20] Lateral variations in thickness increase with the number of deposition pulses as reflected by the error bars.

Several surface limited reactions were used to probe the Ir coverage on Au. H_{UPD} waves for the ultrathin Ir films are stable to voltammetric cycling in 0.5 mol/L H_2SO_4 provided the potential is kept at or below 0.7 V_{RHE} (Fig. 2c). The H_{UPD} charge density increases monotonically with the number of deposition pulses. However, beyond the third Ir deposition pulse the H_{UPD} charge for the Au RDE was larger than that of the Au thin film substrates (Fig. 2c inset). The difference is ascribed to substrate orientation effects on Ir nucleation and growth or to variations in the electrochemical time constant.[6] Complete H occupancy of atop or threefold hollow sites on Ir(111) corresponds to 252 $\mu C/cm_{Ir}^2$. For one deposition pulse films this corresponds to a fractional Ir surface coverage of ≈0.32 (i.e., 0.32 cm_{Ir}^2/cm_{geo}^2).[11-13] After 3 pulses deposition the H_{UPD} coverage approaches a monolayer. In contrast XPS suggests a monolayer is approached after 2 pulses. Furthermore, the H_{UPD} waves are much wider than the narrow peaks on Ir(111) single crystals indicating that the electrodeposited Ir is not in the form of large, well-defined 2-D Ir(111) islands but rather has more in common with Ir(110).[22] The further increase in H_{UPD} charge with subsequent deposition cycles reflects the increasing surface roughness.

The continuity of the Ir overlayers was examined voltammetrically by probing for exposed Au sites via oxide formation and reduction. For Ir deposition on Au thin films less than 10 % of the Au surface remains exposed after 2 deposition cycles (Fig. S17a,d) while 7 deposition pulses are required for a similar coverage on the Au RDE (Fig. S17b,d). These experiments are constrained by substantial rearrangement of the surface due to Au segregation and irreversible Ir oxidation at potentials >0.7 V_{RHE} (Fig. S18,19).[23] The Ir overlayers on Au were also examined using Pb_{UPD} and Cu_{UPD} (Fig. S20). Ir leads to broadening of the sharp UPD peaks associated with respective 2-D phase transitions on 111 textured Au while Pb_{UPD} blocks the H_{UPD} process on Ir. Following multiple Ir deposition pulses the symmetry of the Pb_{UPD} and Cu_{UPD} waves is further weakened. Nevertheless, the Pb_{UPD} and Cu_{UPD} charge increase with the number of Ir deposition pulses analogous to H_{UPD} (Fig. S21).

The structure and morphology of the as-deposited films were examined by high-angle annular dark-field scanning

transmission electron microscopy (HAADF-STEM) and scanning tunneling microscope (STM). The grain size of the Au substrate was similar to the 118 nm film thickness (Fig. S22a). STM reveals the distribution and arrangement of steps (Fig. S22b,c) congruent with the grain size and 111 texture (with possible 180° rotation) of the Au films. The frizzy steps indicate significant step motion accompanies imaging (Fig. 3a). Following 2 deposition pulses, Ir islands ≈(2 to 3) nm in diameter are evident on the Au surface (Fig. 3b). The Ir islands are preferentially associated with highly stepped regions on the Au substrate although significant step motion is still evident on exposed Au regions. Theoretical considerations support Au segregation onto clean Ir surfaces although it remains to be determined how atmospheric exposure and time effect the observed distribution of Ir islands.[23]

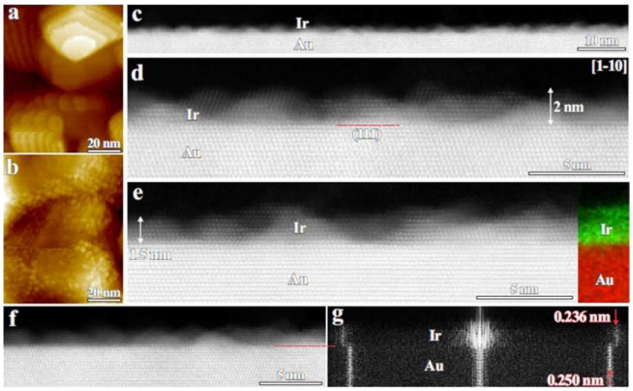

Fig. 3 Microscopic characterization of Ir grwon on Au-seeded Si wafer by multi-pulse deposition in 3 mmol/L K_3IrCl_6-0.5 mol/L Na_2SO_4-x mol/L H_2SO_4 pH 4.0 electrolyte at 70 °C. (a) STM image of 111 textured Au substrate. (b) STM image following 2 pulses Ir deposition on Au showing a distribution of (2 to 3) nm diameter Ir islands. (c-e) HAADF-STEM (110 zone axis) cross section image of a 7 pulses Ir film grown on Au at different magnifications. Examination reveals semi-coherent Ir pyramids as well as a population of islands growing as twins on Au(111) substrate. (e) STEM-XEDS compositional mapping of 7 pulses Ir film (green) on Au (red). (f,g) A HAADF-STEM image and its horizontal 1-d FFT along the [112] showing the abrupt change in the spacing between [1-10] atomic columns reflecting the semi-coherent nature of the interface.

A thicker 7 pulse Ir film was examined by STEM. Atomically-resolved HAADF-STEM imaging reveals a distribution of dense pyramidal Ir islands on the exposed Au(111) surface viewed along the 1-10 (Fig. 3c) and 1-12 zone axis (Fig. S23). The islands range mostly from 1.5 nm to 2.0 nm in height consistent with the (1.7 ± 0.1) nm thickness determined by XPS using a uniform overlayer model.[20] Application of a Volmer-Weber model to the XPS data gives ≈0.12 island/nm^2, assuming uniform hemispherical clusters with a radius equivalent to 8 Ir layers, 1.77 nm.[21] The lateral island dimensions of the 7 pulse Ir films were congruent with the STM images of Ir islands grown using 2 pulses. Lattice alignment between several Ir pyramids and the Au substrate is evident while interface stacking faults yield a significant population of 180° rotated pyramids (Fig. 3d,e). The non-uniform scattering density within a single image along with variation in lattice-resolved imaging of different islands as the focus conditions changed reflect the non-uniform Ir islands distribution on the Au(111) substrate (Fig. S24). The roughness of the Ir layer varied between different regions across the specimen presumably due to variation in substrate step density and accommodation of the lattice misfit. A 1-dimensional FFT in the [112] of the (111) Au/Ir interface shows that the interface is atomically sharp (Fig. 3f,g) with a discrete change in the spacing of the [1-10] atomic columns from 0.236 nm for the Ir islands to 0.250 nm for the Au substrate. Despite the 6.1 % misfit between Ir and Au the islands are minimally strained due to capillarity and step line tension consistent with recent density functional theory (DFT) studies of small diameter, <3 nm, Pt islands on Au(111).[24,25] STEM-XEDS (energy-dispersive X-ray spectroscopy) compositional mapping is congruent with a 2 nm Ir overlayer (Fig. 3e inset).

Hydrogen production and oxidation in alkali solutions (HER/HOR) was examined as a function of the number of Ir deposition pulses. The catalytic activity of the mechanically-polished polycrystalline Pt RDE (Fig. 4a) is in good agreement with prior results while Au is inactive.[3,7,26-28] Ir deposition on the Au RDE results in a monotonic increase in the HOR/HER kinetics with the number of deposition pulses that correlates with the increase in H_{UPD} surface area (Fig. 4b). For Ir films deposited with 3 or more deposition pulses the HOR/HER current exceeds that of the Pt RDE. The HOR specific activity reaches a maximum for Ir films grown using 5 pulses while the maximum specific activity for HER is observed after 3 deposition pulses. The peak in specific activity reflects interactions between Ir, Au, and subsurface H, that favorably affect the HOR/HER in line with recent theoretical suggestions.[29-33] Our results are consistent with a recent report of superior alkaline HOR kinetics for Ir compared to Pt that was attributed to its more oxophilic character although the result and its interpretation have been challenged.[3,28]

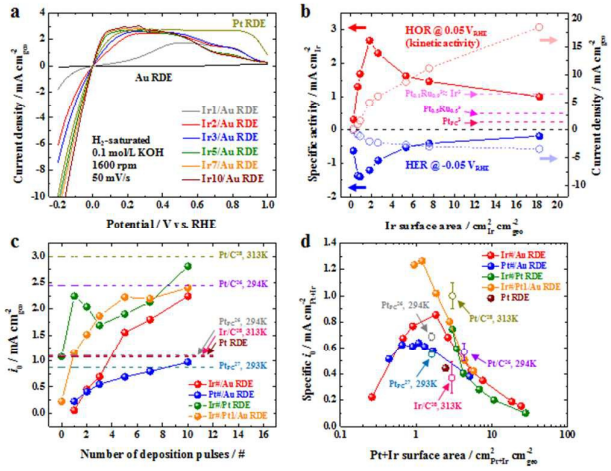

Fig. 4 Alkaline HER/HOR catalysis by self-terminated Ir or Pt layers grown on various substrates. (a) Linear sweep voltammetry (not iR-corrected) for ultrathin Ir films as function of the number of deposition pulses. (b) HER current density (blue) and HOR current density (red) at 50 mV overpotential and normalized to the geometric (open) and Hupd surface area (solid). The dashed line correspond to literature data.[3] (c,d) Exchange current density (calculated from iR-corrected interface charge transfer resistance) for various Ir and/or Pt overlayers on Au or Pt RDE substrates. The exchange current was normalized by (c) geometric and (d) H_{UPD} surface area. Data from literature are shown for comparison (Table S3).[26-28]

The HOR/HER on self-terminated Ir on Pt RDE, self-terminated Pt on Au RDE and Ir/Pt on Au RDE were examined (Fig. 4c, S25). The exchange current density normalized to geometric, H_{UPD} and real surface area is summarized in Fig 4d, S26-29 and Table S2 and compared to literature values for bulk Pt and Ir (Table S3).[26-28] Likewise the iR-corrected HER activity is summarized and compared to literature values in Fig. S30.[7,34] The combination of self-terminated deposition of Ir and Pt give rise to superior HOR/HER performance and demonstrates that the strategy provides a means for rapid synthesis and exploration of multicomponent electrocatalysts.

Water splitting through the oxygen evolution reaction (OER) on ultrathin Ir films was examined in O_2-saturated 0.1 mol/L $HClO_4$ (Fig. 5a). Compared to Pt, water splitting is significantly catalyzed on the ultrathin Ir films with the depolarization increasing with the number of deposition pulse (Fig. 5b, S31). For 3 deposition pulses Ir film, where the H_{UPD} normalized Ir area is roughly equivalent to the projected electrode area, the overpotential at 5 mA/cm^2 is lower than that reported for freshly annealed bulk polycrystalline Ir electrodes (Fig. 5b).[35-37] Further depolarization accompanies the increase in surface roughness associated with the thicker films. Evaluation of the specific OER activity at the thermoneutral potential, 1.48 V, reveals the highest value for the thinnest films, which is more than an order of magnitude greater than that reported for IrO_2 nanoparticles[38] (Fig. 5c, Table S4,5[35-39]). Similar trends were evident at higher potentials.

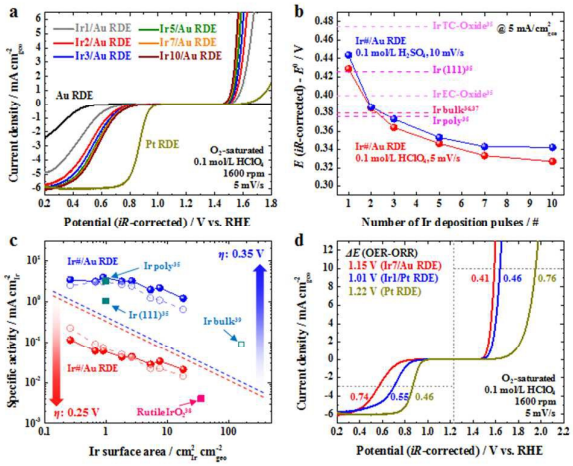

Fig. 5 Acid OER/ORR catalysis by self-terminated Ir or Pt layers grown on various substrates. (a) ORR/OER polarization curves (iR-corrected) for ultrathin Ir films as function of the number of deposition pulses. (b) OER overpotential at 5 mA/cm$_{geo}^2$ for Ir films on a Au RDE in 0.1 mol/L $HClO_4$ (red) and 0.1 mol/L H_2SO_4 (blue). The dashed lines correspond to literature data (Table S4).[35-37] (c) OER specific activity of Ir films on Au RDE at fixed overpotentials, 0.25 V (red) and 0.35 V (blue) in 0.1 mol/L $HClO_4$ (solid) and 0.1 mol/L H_2SO_4 (open) as function of the number of deposition pulses #. Data from literature are shown for comparison (Table S5).[35,38,39] (d) Bifunctional ORR/OER catalysis by Ir7/Au RDE, Ir1/Pt RDE, and Pt RDE.

In contrast to the OER, the oxygen reduction reaction (ORR) on Ir films is quite modest relative to Pt (Fig. 5a,c). However, development of unitized regenerative fuel cells requires improved bifunctional oxygen electrodes (OER/ORR).[40-42] The combination of self-terminated electrodeposition of Ir with Pt yields an improved electrode for regenerative operation (Fig. 5d). This approach opens up a convenient avenue for exploring and optimizing the effects of alloying or composite formation.

Rapid self-terminating electrodeposition reactions provide a new framework for engineering catalytic bimetallic surfaces while minimizing the use of expensive materials. The resulting ultrathin films serve as an excellent materials platform for mechanistic studies of catalysis, whereby most, if not all of the material of interest is directly accessible to the electrolyte offering the prospect of an optimal signal to noise ratio in many cutting edge surface analytical methods.

Acknowledgements

The work was supported by NIST-Materials Measurements Laboratory programs. The X-ray photoelectron spectrometer was provided by NIST-American Recovery and Reinvestment Act funds. NIST has filed a provisional patent application (Atomic Layer Deposition of Ir from Aqueous Solutions) based on this work.

Notes and references

1 M. Carmo, D. L. Fritz, J. Mergel and D. Stolten, *Int. J. Hydrogen Energy*, 2013, **38**, 4901.
2 E. Antolini, *ACS Catal.*, 2014, **4**, 1426.
3 D. Strmcnik, M. Uchimura, C. Wang, R. Subbarman, N. Danilovic, D. Vliet, A. P. Paulikas, V. R. Stamenkovic and N. M. Markovic, *Nat. Chem.*, 2013, **5**, 300.
4 C. C. L. McCrory, S. Jung, I. M. Ferrer, S. M. Chatman, J. C. Peters and T. F. Jaramillo, *J. Am. Chem. Soc.*, 2013, **135**, 16977.
5 J. Hämäläinen, M. Ritala and M. Leskelä, *Chem. Mater.*, 2014, **26**, 786.
6 Y. Liu, D. Gokcen, U. Bertocci and T. P. Moffat, *Science*, 2012, **338**, 1327.
7 Y. Liu, C. M. Hangarter, D. Garcia and T. P. Moffat, *Surf. Sci.*, 2015, **631**, 141.
8 A. Cusanelli, U. Frey, D. T. Richens and A. E. Merbach, *J. Am. Chem. Soc.*, 1996, **118**, 5265.
9 E. N. El Sawy and V. I. Birss, *J. Mater. Chem.*, 2009, **19**, 8244.
10 S. Le Vot, L. Roué and D. Bélanger, *Electrochim. Acta*, 2012, **59**, 49.
11 L.-J. Wan, M. Hara, J. Inukai and K. Itaya, *J. Phys. Chem. B*, 1999, **103**, 6978.
12 T. Senna, N. Ikemiya and M. Ito, *J. Electroanal. Chem.*, 2001, **511**, 115.
13 T. Pajkossy, L. A. Kibler and D. M. Kolb, *J. Electroanal. Chem.*, 2005, **582**, 69.
14 K. A. Soliman, F. C. Simeone and L. A. Kibler, *Electrochem. Commun.*, 2009, **11**, 31.
15 T. Pajkossy, D. M. Kolb, *Russ. J. Electrochem.*, 2009, **45**, 29.
16 I. A. Poulsen and C. S. Garner, *J. Am. Chem. Soc.*, 1962, **84**, 2032.
17 J. C. Chang and C. S. Garner, *Inorg. Chem.*, 1965, **4,** 209.
18 T. M. Buslaeva and S. A. Simanova, *Russ. J. Coord. Chem.*, 1999, **25**, 151.
19 S. Dong, C. Wu, K. Li, Z. Chai, X. Mao and X. Dai, *Anal. Chim. Acta*, 2000, **415**, 185.
20 P. J. Cumpson and M. P. Seah, *Surf. Interface Anal.*, 1997, **25**, 430.
21 U. Diebold, J.-M. Pan and T. E. Madey, *Phys. Rev. B*, 1993, **47**, 3868.

22 S. Motoo and N. Furuya, *J. Electroanal. Chem.*, 1984, **181**, 301.
23 R. L. H. Freire, A. Kiejna and J. L. F. Da Silva, *J. Phys. Chem. C*, 2014, **118**, 19051.
24 S.-E. Bae, D. Gokcen, P. Liu, P. Mohammadi and S. R. Brankovic, *Electrocatal.*, 2012, **3**, 203.
25 J. A. Santana, S. Krüger and N. Rösch, *J. Phys. Chem. C*, 2014, **118**, 22102.
26 W. Sheng, H. A. Gasteiger and Y. Shao-Horn, *J. Electrochem. Soc.*, 2010, **157**, B1529.
27 P. J. Rheinländer, J. Herranz, J. Durst and H. A. Gasteiger, *J. Electrochem. Soc.*, 2014, **161**, F1448.
28 J. Durst, A. Siebel, C. Simon, F. Hasché, J. Herranz and H. A. Gasteiger, *Energy Environ. Sci.*, 2014, **7**, 2255.
29 J. Greeley and M. Mavrikakis, *Nat. Mater.*, 2004, **3**, 810.
30 J. Greeley, T. F. Jaramillo, J. Bonde, I. Chorkendorff and J. K. Nørskov, *Nat. Mater.*, 2006, **5,** 909.
31 P. A. Ferrin, S. Kandoi, J. Zhang, R. Adzic and M. Mavrikakis, *J. Phys. Chem. C*, 2009, **113**, 1411.
32 S. Kandoi, P. A. Ferrin and M. Mavrikakis, *Top. Catal.*, 2010, **53**, 384.
33 D.-H. Seo, H. Shin, K. Kang, H. Kim and S. S. Han, *J. Phys. Chem. Lett.*, 2014, **5**, 1819.
34 R. Subbaraman, D. Tripkovic, D. Strmcnik, K.-C. Chang, M. Uchimura, A. P. Paulikas, V. Stamenkovic, N. M. Markovic, *Science*, 2011, **334**, 1256.
35 N. Danilovic, R. Subbaraman, K.-C. Chang, S. H. Chang, Y. J. Kang, J. Snyder, A. P. Paulikas, D. Strmcnik, Y.-T. Kim, D. Myers, V. R. Stamenkovic, N. M. Markovic, *J. Phys. Chem. Lett.*, 2014, **5**, 2474.
36 T. Reier, M. Oezaslan and P. Strasser, *ACS Catal.*, 2012, **2**, 1765.
37 R. Frydendal, E. A. Paoli, B. P. Knudsen, B. Wickman, P. Malacrida, I. E. L. Stephens and I. Chorkendorff, *ChemElectroChem*, 2014, **1**, 2075.
38 Y. Lee, J. Suntivich, K. J. May, E. E. Perry and Y. Shao-Horn, *J. Phys. Chem. Lett.*, 2012, **3**, 399.
39 C. C. L. McCrory, S. Jung, I. M. Ferrer, S. M. Chatman, J. C. Peters and T. F. Jaramillo, *J. Am. Chem. Soc.*, 2015, **137**, 4347.
40 M. K. Debe, S. M. Hendricks, G. D. Vernstrom, M. Meyers, M. Brostrom, M. Stephens, Q. Chan, J. Willey, M. Hamden, C. K. Mittelsteadt, C. B. Capuano, K. E. Ayers and E. B. Anderson, *J. Electrochem. Soc.*, 2012, **159**, K165.
41 J. M. Roller, M. J. Arellano-Jiménez, R. Jain, H. Yu, C. B. Carter and R. Maric, *J. Electrochem. Soc.*, 2013, **160**, F716.
42 T. C. Crowtz, D. A. Stevens, R. J. Sanderson, J. E. Harlow, G. D. Verstrom, L. L. Atanasoska, G. M. Haugen, R. T. Atanasoski and J. R. Dahn, *J. Electrochem. Soc.*, 2014, **161**, F961.

Broader context:

Development of a sustainable hydrogen economy based on water electrolysis and fuel cells is constrained by the performance, longevity and high cost of Pt group electrocatalysts. Important strategies for improving catalytic reactivity include alloying, forming bimetallic or alloyed surfaces, and engineering substrate-catalyst interactions. At the same time, significant effort is underway to minimize the loading of Pt group metals by examining new synthesis methods and electrode geometries. Of particular interest is atomic layer deposition for growing ultrathin films that maximize utilization of rare, expensive metals and facilitate the exploration of bimetallic effects in electrocatalysis. Among the Pt group metals, Ir is the rarest and it is also the best known elemental catalysts for the oxygen evolution reaction (OER) in acid environments and the production (HER) and oxidation (HOR) of hydrogen in alkaline media. Herein a rapid, inexpensive "wet" atomic layer deposition process is introduced that takes advantage of self-terminated Ir electrodeposition to enable the fabrication of ultrathin Ir films on Au, Pt and Ni substrates. The monolayer equivalent Ir films are found to match the best known specific OER and HER/HOR activity for bulk polycrystalline Ir electrodes thereby increasing the scalability of this important precious metal in energy conversion devices.